1.0

4.5
5.0
5.6
6.3

2.8

2.5

3.2

2.2

3.6

1.1

4.0

2.0

1.8

1.25

1.4

1.6

MICROCOPY RESOLUTION TEST CHART

NATIONAL BUREAU OF STANDARDS-1963-
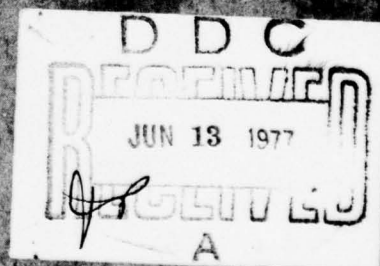
RM-630

A STUDY OF STRUCTURAL
FAILURE MODES FOR A
COMPUTER CRASH SIMULATION

March 1977

RESEARCH DEPARTMENT

GRUMMAN AEROSPACE CORPORATION
BETHPAGE NEW YORK

REPORT DOCUMENTATION PAGE		READ INSTRUCTIONS BEFORE COMPLETING FORM
1. REPORT NUMBER RM-630	2. GOVT ACCESSION NO.	3. RECIPIENT'S CATALOG NUMBER
4. TITLE (and Subtitle) A Study of Structural Failure Modes for a Computer Crash Simulation		5. TYPE OF REPORT & PERIOD COVERED Memorandum
		6. PERFORMING ORG. REPORT NUMBER RM-630
7. AUTHOR(s) R. Winter		8. CONTRACT OR GRANT NUMBER(s) N/A
9. PERFORMING ORGANIZATION NAME AND ADDRESS Grumman Aerospace Corporation		10. PROGRAM ELEMENT, PROJECT, TASK AREA & WORK UNIT NUMBERS N/A
11. CONTROLLING OFFICE NAME AND ADDRESS N/A		12. REPORT DATE March 1977
		13. NUMBER OF PAGES 61
14. MONITORING AGENCY NAME & ADDRESS(if different from Controlling Office) N/A		15. SECURITY CLASS. (of this report) Unclassified
		15a. DECLASSIFICATION/DOWNGRADING SCHEDULE
16. DISTRIBUTION STATEMENT (of this Report) Approved for Public release; distribution unlimited		
17. DISTRIBUTION STATEMENT (of the abstract entered in Block 20, if different from Report) N/A		
18. SUPPLEMENTARY NOTES N/A		
19. KEY WORDS (Continue on reverse side if necessary and identify by block number)		
20. ABSTRACT (Continue on reverse side if necessary and identify by block number)		

The failure modes of a stiffened skin structure, built-up
from beams, stringers, frames, and panels, under a single con-
tinuously increasing deformation event are:

over

DD FORM
1 JAN 73 1473   EDITION OF 1 NOV 65 IS OBSOLETE
S/N 0102-014-6601

Material (Separation) Failures,

    o   Rupture and tearing (no flaws),

    o   Fracture (with flaws), and

    o   Connection (fastener) failures;

Geometric (Deformation) Failures,

    o   Plastic collapse, and

    o   Elastic buckling.

This document reviews the physical aspects of these failure modes, examines some ways of implementing them in the Dynamic Crash Analysis of STructures (DYCAST) modules of the PLANS computer codes, and makes recommendations and suggestions for implementation.

Grumman Research Department Memorandum RM-630

A STUDY OF STRUCTURAL FAILURE MODES
FOR A COMPUTER CRASH SIMULATION.

by

R. Winter

Materials and Structural Mechanics

Memorandum rept.,

March 1977

65p.
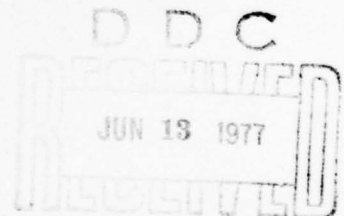
Approved by: *Richard A. Scheuing*
Richard A. Scheuing
Director of Research
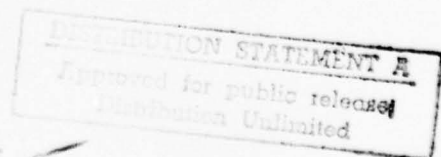
ABSTRACT

The failure modes of a stiffened skin structure, built-up from beams, stringers, frames, and panels, under a single continuously increasing deformation event are

Material (Separation) Failures

- Rupture and tearing (no flaws)
- Fracture (with flaws)
- Connection (fastener) failures

Geometric (Deformation) Failures

- Plastic collapse
- Elastic buckling

This document reviews the physical aspects of these failure modes, examines some ways of implementing them in the DYnamic Crash Analysis of STructures (DYCAST) module of the PLANS computer codes, and makes recommendations and suggestions for implementation.

ii

TABLE OF CONTENTS

iii

LIST OF ILLUSTRATIONS

1. INTRODUCTION

The DYCAST code is the dynamic analysis module of the PLANS (Plastic Large deflection Analysis of Structures) system of computer codes. It predicts the history of mechanical behavior of an aircraft structure under dynamic loading conditions. Given the proper stress-strain curves for each material used in the structure, the code predicts the change in deformations, strains, stresses, and loads developed in any time increment, based on the current shape and stiffness of the structure at the start of that increment. Thus, a piece-wise linear approximation of the nonlinear, elastic plastic, large deformation, dynamic structural behavior is calculated. With certain limitations, this method will predict the collapse of a structure due to plasticity, that is, due to progressive loss of material stiffness as stress and strain levels increase. The effect of the changing geometry in either increasing or decreasing the stiffness is also accounted for during the collapse. The treatment of combined material and geometric nonlinearities as available in DYCAST is similar to the procedures used in other PLANS modules and described in Ref. 1.

Without any material failures involving separation of material (rupture, tearing, fracture) the structure will dissipate energy by means of plastic deformation as each component proceeds along its particular load-deformation curve, as indicated by path oabcd in Fig. 1a. Under these conditions it is implied that the material will have unlimited strain capability, and each element will deform until it is unloaded, or until some arbitrary geometric limit is reached.

Figure 1a also shows the different characteristics of load-shedding and finite strain energy dissipation in an element. The unloading by reduction of external forces proceeds initially along

1
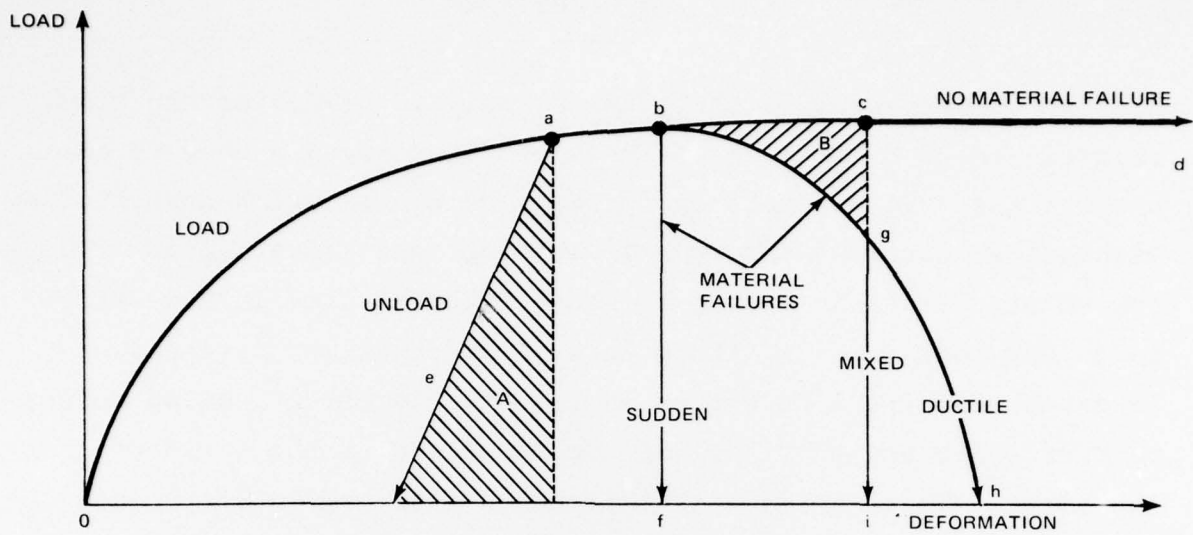
a) Single-Component Behavior
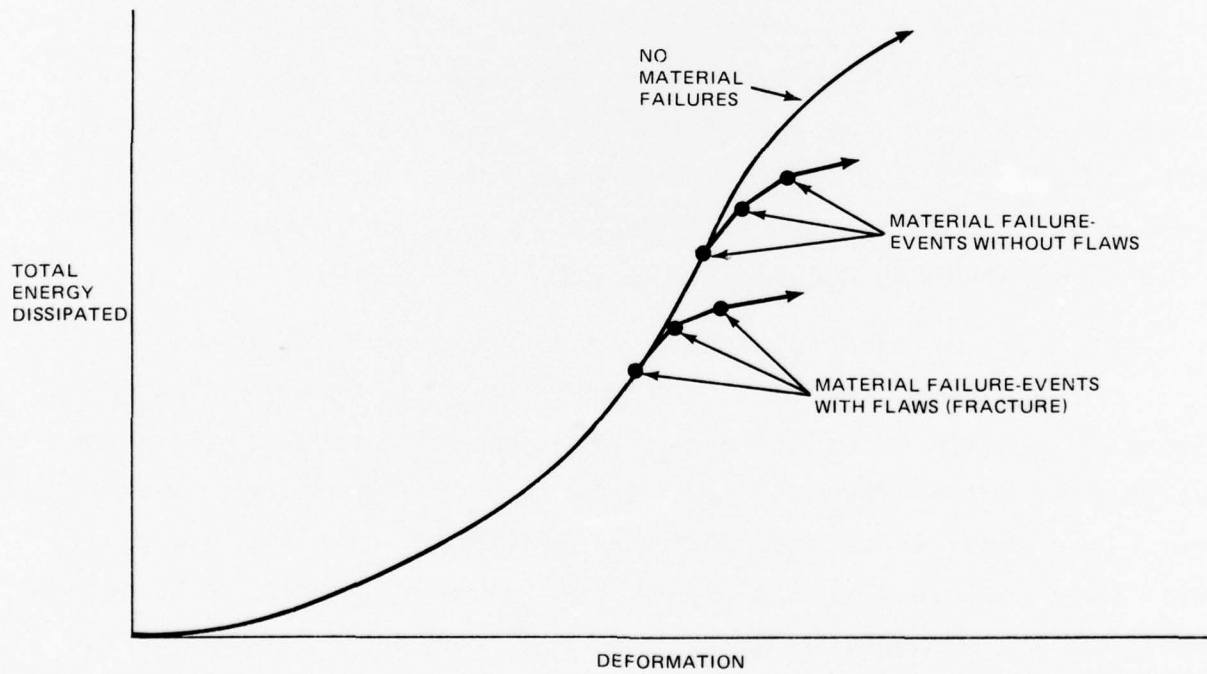
b) Multiple-Component Redundant Structural Behavior

Fig. 1 Structural Behavior Characteristics

2

an elastic line, so that at least the elastic energy (Region A) stored at the maximum external load is returned to the system when material failure does not occur. When a purely brittle material failure occurs none of the stored energy is returned to the structural system, if we assume a sudden and complete separation of the cross section of the component. The external load then drops to zero at constant displacement of the component's attachment points (path oabf). For a purely ductile failure, the load is shed over a range of deformation, as "necking" (localized thickness reduction) develops, while the component continues to absorb energy (path oabgh). Many structural materials exhibit a mixed failure mode, in which a sudden failure follows some amount of ductile necking (path oabgi). In this case it is convenient to assume that a sudden failure occurred at the critical deformation (path oabcgi), even though this will overestimate the energy absorbed by the amount of Region B, and this last failure model is suggested.

Most unflawed structural components will fail suddenly at some finite level of deformation or load, and each component failure reduces the additional energy that can be absorbed by the structure, as indicated in Fig. 1b. This figure distinguishes between material failures without flaws, such as rupture and tearing, and fracture with existing flaws or cracks. The presence of flaws will further lower the failure loads of the components, and therefore the total energy absorbed by the structure is further reduced. If the material has a low fracture toughness, the reduction due to flaws can be large. For a high fracture toughness, the reduction may be negligible.

3

2. MATERIAL FAILURES

Material failures are characterized by separation of material. Three types of failure are considered here:

- Rupture - a sudden separation through the entire cross section of a member

- Tearing - in a skin panel, a separation that begins at one edge and passes through the panel toward another edge

- Fracture - extension of an existing crack or flaw through the entire cross section of a member, thus causing failure

Usually, structural materials will have limited ductility, so that plastic deformation is possible only up to a critical strain level ϵ_f, at which a material failure will occur. In the case of a structural element under tension strain through a cross section, sudden and complete failure will occur at the ultimate, or critical, strain level. For components in which bending dominates, failure will also be complete if constant loads and moments are maintained. In a highly redundant structure, with multiple load paths, such a component may not fail completely, because it will be quickly relieved of all its load by the surrounding structure as its stiffness drops. In any case, complete and permanent load shedding will occur.

Thus, it seems likely that when the material failure strain is reached at any point in an element or component under a continuously increasing deformation, that element will no longer be able to carry load or absorb additional energy. This can be simulated by setting its stiffness to zero (or numerically close to zero).

The failure is now a material failure in the brittle mode, even though large plastic strains might have previously occurred, as indicated in Fig. 1a.

RUPTURE AND TEARING

Isotropic Materials

It will be assumed that tearing and rupture are different manifestations of the same material failure process; that regardless of previous plastic strains, they are brittle failure modes. Brittle failure has been analyzed by several methods; the most convenient one for these purposes is the (St. Venant) maximum principal strain theory, which states that failure occurs at a point in an isotropic structure when the maximum principal tension strain equals the failure strain achieved in a simple tension test. In practice, the general application of this theory requires that the principal strains be found in every finite element of the structure. However, calculations could be limited, if desired, to certain selected critical elements.

In general, the principal strains $\epsilon_1, \epsilon_2, \epsilon_3$ are the three roots of the equation (Ref. 2, p. 18, for example)

$$\epsilon^3 - I_1 \epsilon^2 - I_2 \epsilon - I_3 = 0 \tag{1}$$

The coefficients are the three strain invariants

$$I_1 = \epsilon_x + \epsilon_y + \epsilon_z \tag{2}$$

$$I_2 = \epsilon_{xy}^2 + \epsilon_{yz}^2 + \epsilon_{zx}^2 - (\epsilon_x \epsilon_y + \epsilon_y \epsilon_z + \epsilon_z \epsilon_x) \tag{3}$$

$$I_3 = \epsilon_x \epsilon_y \epsilon_z + 2\epsilon_{xy} \epsilon_{yz} \epsilon_{zx} - (\epsilon_x \epsilon_{yz}^2 + \epsilon_y \epsilon_{zx}^2 + \epsilon_z \epsilon_{xy}^2) \tag{4}$$

5

where the $\epsilon_x, \epsilon_{xy}.$ etc., are the strain components in the local coordinate system. The solution (see Ref. 3, for example) is then

$$\epsilon_k = 2 \sqrt{-\left(\frac{a}{3}\right)} \cos\left[\frac{\phi}{3} + \frac{2\pi}{3} k\right] \quad , \quad k = 1, 2, 3 \tag{5}$$

where

$$\phi = \text{arc } \cos \sqrt{-\left(\frac{b}{2}\right)^2 \left(\frac{3}{a}\right)^3} \tag{6}$$

and

$$a = -\frac{1}{3} (I_1^2 + 3I_2) \tag{7}$$

$$b = -\frac{1}{27} (2I_1^3 + 9I_1 I_2 + 27I_3) \tag{8}$$

Thus, for the general state of three dimensional strain

$$\epsilon_k = \frac{2}{3} \sqrt{I_1^2 + 3I_2} \cos\left(\frac{\phi}{3} + \frac{2\pi}{3}k\right) \quad , \quad k = 1, 2, 3 \tag{9}$$

where

$$\phi = \text{arc } \cos\left|\frac{2I_1^3 + 9I_1 I_2 + 27I_3}{2(I_1^2 + 3I_2)^{3/2}}\right| \tag{10}$$

For most structural metals, a sufficient amount of plasticity will develop prior to the material failure, so that the volumetric (dilational) strain will be small compared to the distortional (deviatoric) strain.

We now have

$$\frac{\Delta v}{v} = \epsilon_x + \epsilon_y + \epsilon_z = I_1 = 0 \tag{11}$$

so that

$$\epsilon_z = - (\epsilon_x + \epsilon_y) \tag{12}$$

Therefore

$$I_2 = \epsilon_{xy}^2 + \epsilon_{yz}^2 + \epsilon_{zx}^2 + \epsilon_x^2 + \epsilon_y^2 + \epsilon_x\epsilon_y \tag{13}$$

$$I_3 = -\epsilon_x(\epsilon_y^2 + \epsilon_{yz}^2 - \epsilon_{xz}^2) - \epsilon_y(\epsilon_x^2 + \epsilon_{zx}^2 - \epsilon_{xy}^2) + 2\epsilon_{xy}\epsilon_{yz}\epsilon_{zx} \tag{14}$$

$$\epsilon_k = \frac{2\sqrt{3}}{3}\sqrt{I_2}\,\cos(\frac{\phi}{3} + \frac{2\pi}{3}k) \quad , \quad k = 1,\,2,\,3 \tag{15}$$

$$\phi = \text{arc } \cos\left|\frac{3\sqrt{3}}{2}\,\frac{I_3}{I_2^{3/2}}\right| \tag{16}$$

At a free surface, the transverse shear strains must vanish. Therefore, for thin surface-type structural elements, such as membranes, plates, shear panels, and the webs and flanges of thin-walled stiffeners, commonly found in airplanes, the transverse shear strains can usually be neglected. Thus, for the z-axis normal to the element surface, $\epsilon_{zx} = \epsilon_{yz} \approx 0$ and

$$I_2 = \epsilon_{xy}^2 + \epsilon_x^2 + \epsilon_y^2 + \epsilon_x\epsilon_y \tag{17}$$

$$I_3 = -\epsilon_x(\epsilon_y^2 - \epsilon_{xy}^2) - \epsilon_y(\epsilon_x^2 - \epsilon_{xy}^2) \tag{18}$$

The principal strains can then be found from Eq. (15) through Eq. (18).

For a one dimensional structural element such as a beam or column under combined axial force, bending moments, and torsion, where x is the longitudinal axis, $\epsilon_y = \epsilon_z = -\nu\epsilon_x = -\frac{1}{2}\epsilon_x$, and $\epsilon_{yz} = 0$. Note that Eq. (11) requires the effective Poisson's ratio, ν, be $\frac{1}{2}$, which pertains to the condition when plastic strain is large compared to elastic strain. Then,

$$I_2 = \epsilon_{xy}^2 + \epsilon_{zx}^2 + \frac{3}{4}\epsilon_x^2 \qquad (19)$$

$$I_3 = \epsilon_x(\tfrac{1}{4}\epsilon_x^2 + \epsilon_{xy}^2 + \epsilon_{zx}^2) \qquad (20)$$

The principal strains can be found from Eqs. (15), (16), (19), and (20). For a simple axial loading element such as a stringer, $\epsilon_y = \epsilon_z = -\frac{1}{2}\epsilon_x$, and $\epsilon_{xy} = \epsilon_{yz} = \epsilon_{zx} = 0$. The normal coordinate strains $\epsilon_x, \epsilon_y, \epsilon_z$ are now the principal strains, by definition. Using the previous formulas, Eqs. (15), (16), and 20), we have $I_2 = \frac{3}{4}\epsilon_x^2$, $I_3 = \frac{1}{4}\epsilon_x^3$, and $\phi = \text{arc } \cos(1) = 0$. So that $\epsilon_k = \frac{2}{3}\sqrt{\frac{9}{4}\epsilon_x^2} \cos\frac{2\pi}{3} k = \epsilon_x \cos\frac{2\pi}{3} k$; $\quad k = 1, 2, 3$. This gives, for the principal strains,

$$\epsilon_1 = \epsilon_x \cos\frac{2\pi}{3} = \epsilon_x \cos 120° = \epsilon_x(-\cos 60°) = -\tfrac{1}{2}\epsilon_x$$

$$\epsilon_2 = \epsilon_x \cos\frac{4\pi}{3} = \epsilon_x \cos 240° = \epsilon_x(-\cos 60°) = -\tfrac{1}{2}\epsilon_x$$

$$\epsilon_3 = \epsilon_x \cos 2\pi = \epsilon_x$$

as was expected.

Thus, for isotropic bodies the failure criterion is met whenever

$$\epsilon_{k_{max}} \geq \epsilon_f \quad , \qquad k = 1, 2, 3 \qquad (21)$$

or, defining a "material failure function" f, failure occurs whenever

$$f = \epsilon_{k_{max}} - \epsilon_f \geq 0 \qquad (22)$$

This function can be visualized more generally by considering a surface in the coordinate space at a point, which surface describes

8

the end point of the tension failure strain vector in every direction. Consider a second surface that describes the end point of all the applied normal tension strain vectors in every direction. This applied strain surface grows as the external loading or deformation on the element increases. When the applied strain surface touches the failure strain surface, material failure occurs in the direction of the vector to the contact point.

The maximum tensile strain at a point in a body is always one of the principal strains. In an isotropic body, the failure strain surface is always a sphere, therefore, the failure will occur in an isotropic body when the maximum principal tension strain equals the failure strain. A single uniaxial tension test is sufficient to determine the failure surface in an isotropic material.

Anisotropic Materials

In an anisotropic body, the failure strain surface is nonspherical. Failure will occur when any point on the applied strain surface reaches the failure strain surface. In this case, the critical strain need not be the maximum principal strain, or any principal strain.

The applied normal strain in any direction at a point is characterized by (see Ref. 4, p. 40, for example)

$$\epsilon = \ell_x^2 \epsilon_x + \ell_y^2 \epsilon_y + \ell_z^2 \epsilon_z + 2\ell_x \ell_y \epsilon_{xy} + 2\ell_y \ell_z \epsilon_{yz} + 2\ell_z \ell_x \epsilon_{zx} \tag{23}$$

where the ℓ_x, ℓ_y, ℓ_z are the direction cosines from the coordinate axes to the direction of interest as follows:

$$\ell_x = \cos \alpha \tag{24}$$

$$\ell_y = \cos \beta \tag{25}$$

$$\ell_z = \cos \gamma \tag{26}$$

9

The angles α, β, γ are between the direction of interest and the three coordinate axes, x,y,z, respectively.

For a generally anisotropic material, the failure strain surface can have any shape depending on the material's internal configuration. Therefore, a complete representation of its failure characteristics would require failure test data at sufficient orientations in the material to construct mathematically this surface.

However, it is possible to construct a simple approximation to the actual failure strain surface. An orthotropic material has three mutually perpendicular planes of symmetry. The measured failure strains in the three orthotropic directions are defined as $\epsilon_{1_f}, \epsilon_{2_f}, \epsilon_{3_f}$. Arbitrarily treating these three failure strains as if they were principal strains, one can get an equation for the failure strain in any direction, describing a presumed failure surface, i.e.,

$$\epsilon_f = m_1^2 \epsilon_{1_f} + m_2^2 \epsilon_{2_f} + m_3^2 \epsilon_{3_f} \tag{27}$$

where the m_1, m_2, m_3 are the direction cosines from the direction of interest to the axes of orthotropy. This surface is not exactly correct, except in the three directions of orthotropy, but is used here for convenience. It is assumed to be a reasonable approximation on the grounds that the three orthotropic failure strains are local maxima and minima of the failure strain surface, and that any smooth connection between them is a reasonable first approximation.

The material failure criterion is now expressed mathematically as

$$f \equiv \epsilon - \epsilon_f \geq 0 \tag{28}$$

where the individual terms are given in Eqs. (23) and (27). Note that the applied normal strain ϵ in any direction is given as a function of the coordinate strains and the angles to the coordinate axes, while the failure strain ϵ_f in the same direction is stated as a function of the orthotropic failure strains and the angles to the orthotropic axes. Geometrically, f is the distance between the failure surface and the applied strain surface in any direction at a point.

Usable Data

The question arises as to what values of ϵ_f are to be used in the failure criterion. DYCAST calculates the increment of displacement, ΔL, during a time interval by using the previous deformed state as the initial shape. Therefore, the incremental strain of any line of current length L in the structure is

$$\Delta \epsilon = \frac{\Delta L}{L} \tag{29}$$

The total accumulated strain at any time is

$$\epsilon = \sum_{L=L_o}^{L} \frac{\Delta L}{L} \tag{30}$$

which approximates the true strain (also called the natural or logarithmic strain) defined as

$$\epsilon = \int_{L_o}^{L} \frac{dL}{L} = \ln \frac{L}{L_o} = \ln\left(1 + \frac{L - L_o}{L_o}\right) = \ln\left(1 + \frac{\Delta L}{L_o}\right) \tag{31}$$

11

where $\Delta L/L_o$ is the usually measured engineering strain, based on the initial length L_o.

Since DYCAST approximates true strains in its calculations, all its strain data inputs should ideally be in true strain units. Thus, the true failure strain ϵ_f is to be used in the failure criterion and is related to the engineering failure strain $(\Delta L/L_o)_f$ by

$$\epsilon_f = \ln \frac{L_f}{L_o} = \ln\left[1 + (\Delta L/L_o)_f\right] \qquad (32)$$

Measured failure strains from tension tests are usually given as the average value of $\Delta L/L_o$ over a given gauge length L_o (for example, "25 percent elongation in 2 inches"). When the strain is uniform over the gauge length up to failure, the stated value can be used directly in the above Eq. (32). This is usually the case for materials having little or no ductility (little or no plastic strain before failure).

However, in the case of ductile materials exhibiting significant plastic strains before failure, the strain distribution in the gauge length at failure is often very nonuniform. The region of highest strain is often confined to a short band or necking region, in which the maximum strain is much greater than the stated average value over the gauge length. This is essentially a plane stress phenomenon, occurring near a free surface in the material, and is most common in thin sections.

In some cases, the reduction of area is given at the failure section. For large plastic strains, the incompressible material assumption is valid, and the deformation takes place at constant volume. The volume in the necked-down portion is

12

$$L_o' A_o = L_f' A_f \qquad (33)$$

where L_o' and L_f' are the initial and final lengths of the necked-down section and A_o and A_f are the corresponding values of the cross sectional area. Thus

$$\frac{L_f'}{L_o'} = \frac{A_o}{A_f} \qquad (34)$$

and so the true local failure strain in the necked portion becomes

$$\epsilon_f' = \ln \frac{L_f'}{L_o'} = \ln \frac{A_o}{A_f}$$

$$= \ln \frac{A_o}{A_o + \triangle A_f} = \ln \frac{1}{1 + \left(\frac{\triangle A}{A_o}\right)_f}$$

$$\epsilon_f' = - \ln \left[1 + \left(\frac{\triangle A}{A_o}\right)_f \right] \qquad (35)$$

where $\left(\triangle A / A_o\right)_f$ is the so-called "reduction in area" (a negative number less than unity) at failure in the necked region.

The values of average true failure strain and local true failure strain, from Eqs. (32) and (35), are listed for several structural metals in Table 1. Note that these two failure strain values are nearly the same for low failure strains (brittle metals), indicating uniform strain at failure, and are very different for high failure strains (more ductile metals), indicating local necking at failure. The local failure strain is greater than or equal to the average failure strain, and the ratio of these two strains is a measure of the nonuniformity in strain distribution in uniaxial tension tests. This ratio is listed in the last column of Table 1.

13

TABLE 1 TYPICAL FAILURE STRAINS

Material	Typical Failure Elongation in 2 In. $(\Delta L/L_o)$	Typical Reduction of Area $(\Delta A/A_o)$	Average Longitudinal True Failure Strain $\bar{\epsilon} = \ln[1+\Delta L/L_o]$	Local True Failure Strain[†] $\epsilon' = -\ln[1+\Delta A/A_o]$	$\epsilon'/\bar{\epsilon}$
Aluminum					
2024-T4	0.12	0.10-0.15	0.11	0.11-0.16	1.0-1.5
7075-T6	0.13	0.23	0.12	0.26	2.2
Steel					
Stainless 302 annealed	0.60	0.70	0.47	1.20	2.5
Stainless 302 cold worked	0.35	0.60	0.30	0.92	3.1
Cast 60 ksi annealed	0.30	0.54	0.26	0.78	3.0

† In "necked" region

14

Theoretical predictions of elastic-plastic strains in DYCAST are based on the assumption of a homogeneous material, and this applies up to and including the failure point. The more brittle materials, with their nearly uniform strain distribution at failure, will follow this assumption quite well, and their failure test data can be used directly to calculate ϵ_f by either of Eqs. (32) or (35). The elongation-to-failure method of Eq. (32) is preferred because the measurement accuracy is better.

For the more ductile materials, exhibiting large nonuniformities of strain in test samples, the local strain, Eq. (35), will be too large, depending on measurements taken entirely from the necked region. The average longitudinal strain, Eq. (32), will also overestimate the strain in the unnecked region, but by a much smaller error. The actual error will depend on the necked length and the average strain in the necked region. Expressed mathematically, the error using the average longitudinal strain at failure is

$$\frac{\bar{\epsilon} - \epsilon_o}{\epsilon_o} = \frac{\epsilon' L' + \epsilon_o (L_o - L')}{L_o \epsilon_o} - 1 = \frac{L'}{L_o} \left(\frac{\epsilon'}{\epsilon_o} - 1 \right) \qquad (36)$$

where $\bar{\epsilon} = \Delta L / L_o$, the measured average strain, ϵ' and ϵ_o are the strains in the necked and unnecked portions, and L' and L_o are the necked length and the total gauge length. If the effective necking strain is twice that of the unnecked portion, and the necked length is 10 percent of the gauge length (0.2 in. in a 2 in. gauge length), then the error will be +10 percent. It can be seen from Eq. (36) that the error in the average strain will decline as the gauge length increases, since the necking is fixed for a given diameter.

In conclusion, it seems that the best available procedure would be to use the average elongation-to-failure as $\Delta L / L_o$ in Eq. (32) to calculate the true failure strain ϵ_f, for use in the

15

material failure criterion, Eqs. (33) or (28). With this method, the effects of local yielding can be minimized when the average strain data are measured over the largest possible gauge length. This method tends to be more compatible with the usual theories of structural analysis, which assume uniform strains under uniform stress. The reduction in area method of Eq. (35) maximizes the effect of the local yielding and therefore will greatly overestimate the required failure strain, and is not compatible with the conventional continuum mechanics theory. Furthermore, since the extent of nonuniform strain depends on the thickness of the sample or component, the failure strain data should ideally be taken from samples having the same thickness as the structural component to be analyzed. This applies to the stress-strain curve as well, but not as strongly, because only the final stages near failure are affected by nonuniform strains.

FRACTURE

The existence of a flaw or crack of any size in a structural member will tend to reduce the effective ultimate strength of the member compared to the strength derived from uniaxial tests on unflawed specimens. The more brittle materials, with low fracture toughness values, may be significantly affected by even small flaws while the more ductile materials may not be affected by relatively large flaws. The prediction of the failure conditions in any general structural member requires that the existing or probable flaw or crack sizes in the member be known or assigned arbitrarily, and that the local stress intensity at the flaw be monitored.

The mathematical theory and engineering applications of fracture mechanics can be found in many reference works (see Ref. 5),

16

and will not be discussed here. It will be sufficient to note that the local elastic stress components in the neighborhood of a crack tip all have the form

$$\sigma(r,\theta) = \frac{K}{\sqrt{2\pi r}} \, f(\theta) \qquad (37)$$

where r, θ are the radial and angular coordinates from the crack tip, and K is a factor that depends on the type and magnitude of the external load, size of the flaw, and shape of the member in the vicinity of the crack tip. The factor K then determines the magnitude of the stress components for a given load and shape, and is termed the "stress intensity factor."

The calculated stress intensity factors K, induced by the applied loads, can then be compared to their critical values K_c, also known as the "fracture toughness." When any K reaches or exceeds its critical value K_c, the existing flaw or crack will become unstable, and will propagate through the member until stopped by a crack arresting feature, or until complete failure of the member occurs.

Three types of crack behaviors have been identified, as shown in Fig. 2a. In general, the stress intensity factors can be expressed as

$$K_1 = C_1 \sqrt{a} \, \sigma \qquad (38)$$

$$K_2 = C_2 \sqrt{a} \, \tau \qquad (39)$$

$$K_3 = C_3 \sqrt{a} \, \tau' \qquad (40)$$

where a is a representative dimension of the crack length (as shown in Fig. 2b, σ, τ, and τ' are the local ambient stress levels that would prevail at the site if no flaw were present,

17
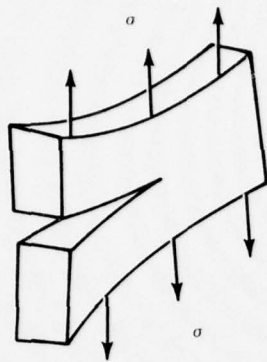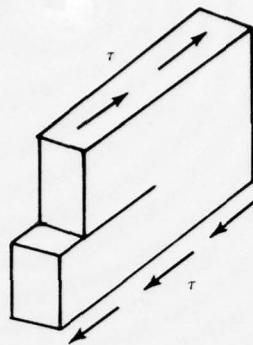
MODE I

TENSION

MODE II

IN-PLANE SHEAR
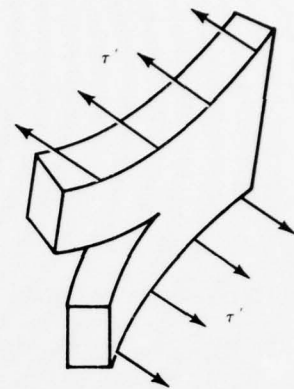
MODE III

OUT-OF-PLANE SHEAR

a) Fracture Deformation Modes
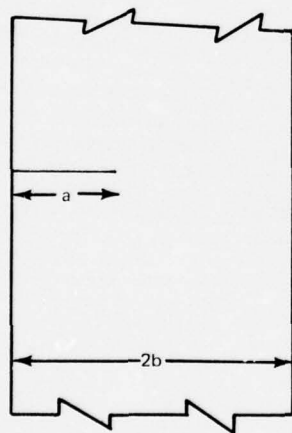
EDGE CRACK
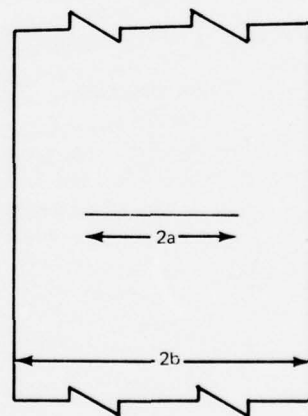
INTERIOR CRACK

b) Flaws in Thin Elements

Fig. 2 Crack Geometry

18

and C is a dimensionless factor depending on the type of loading, the existing flaw or crack shape, and the member shape.

Formulas and tables for values of C in many practical cases are available in the literature (for example, Reg. 6). For typical aircraft construction, using thin skin panels, and stiffeners made of thin flanges and webs, two types of flaws or cracks seem most applicable. They are the interior central crack and the edge crack in a thin plate, both completely through the thickness, as shown in Fig. 2b. Approximate values of K for these two cases are given in Table 2.

Mode III is not presented since transverse shear stresses are negligible for thin elements and are therefore not calculated in DYCAST.

TABLE 2   STRESS INTENSITY FACTORS

Stress Intensity Factor	Edge Crack	Interior Crack
K_1 (tension)	$\sqrt{2b \tan(\pi a/2b)}\ \sigma$	$\sqrt{2b \tan(\pi a/2b)}\ \sigma$
K_2 (shear)	$\sqrt{2b \tan(\pi a/2b)}\ \tau$	$\sqrt{2b \tan(\pi a/2b)}\ \tau$

The term $2b \tan(\pi a/2b)$ in Table 2 inside the square root was developed by Paris and Sih (Ref. 6). It differs only slightly in value from the commonly used expression $\pi a \sec(\pi a/2b)$, cited in MIL-HDBK-5B, Chapter 9 (Ref. 7). When $a/b = 0.5$, for example, Table 2 will produce a value of K only 5 percent smaller than

19

that indicated in MIL-HDBK-5B. For very small cracks, $a/b \to 0$, the two values of K become equal. Paris and Sih also indicate that the K for a short crack at a free edge is about 12 percent larger than that for a long edge crack or a center crack, but this factor has been neglected.

The failure condition is then

$$K \geq K_c \tag{41}$$

where K_c are the measured fracture toughness values for the material, applied to the three cases of Table 2. When these conditions are met, the member should be assumed to have completely failed. These fracture toughness values are often dependent on the thickness of the material, especially for the thin sections used in aircraft. Test data have shown that the K_c values are independent of member geometry only when plane strain conditions exist, and when the plastic zone at the crack tip is far from a boundary. It has been estimated that these conditions require that the dimensions be greater than approximately 50 times the size of the plane strain plastic zone at the crack tip. That is, the thickness, width, etc., must exceed $2.5(K_c/\sigma_y)^2$, where σ_y is the yield strength of the material (Ref. 8). This is because the plastic zone at a real crack tip must be small compared to any dimension in the member in order for the purely elastic model of linear fracture mechanics to apply accurately. Measured values of fracture toughness taken from sufficiently thick test specimens are called Plane Strain Fracture Toughnesses, K_I and K_{II}, and are considered to be true material properties. They are the minimum values of fracture toughness for a material.

In the case of aircraft construction, the plate, stiffener, and beam sections are usually too thin for the plane strain conditions to apply, and their effective toughness values will often be greater than the plane strain fracture toughnesses for the material. The effective values K_{1_c} and K_{2_c} are then dependent on the thickness, and care should be taken to use the K_c value pertaining to each thickness. Using the plane strain fracture toughness values might significantly underestimate the fracture strength of a thin component.

In the application of this failure criterion, the arbitrary stress state, at a point where a flaw is assumed to exist, is calculated without the flaw, as usual. This becomes the ambient stress state, which is presumed to be disturbed only locally by the introduction of the flaw and its stress concentrations. The size of the disturbed region, for thin elements, will be larger than the plane stress plastic zone size, $0.15 \ (K_c/\sigma_y)^2$, and probably smaller than the minimum dimension recommended for fracture test specimens (by the ASTM Fracture Committee Ref. 8), $2.5(K_c/\sigma_y)^2$. It is assumed that sufficiently distant from the flaw, the ambient stress state is not significantly disturbed. These calculations will not apply accurately when the crack is placed into a region where the ambient "unflawed" stress state changes greatly over the crack-disturbed region.

In plate or membrane elements, the ambient stress state must be resolved into stresses normal to and tangential to the crack, corresponding to the mode I normal stress and the mode II shear stress. For a two dimensional stress state in a thin element, with the geometry shown in Fig. 3, the transformation equations (from Mohr's circle) are

21
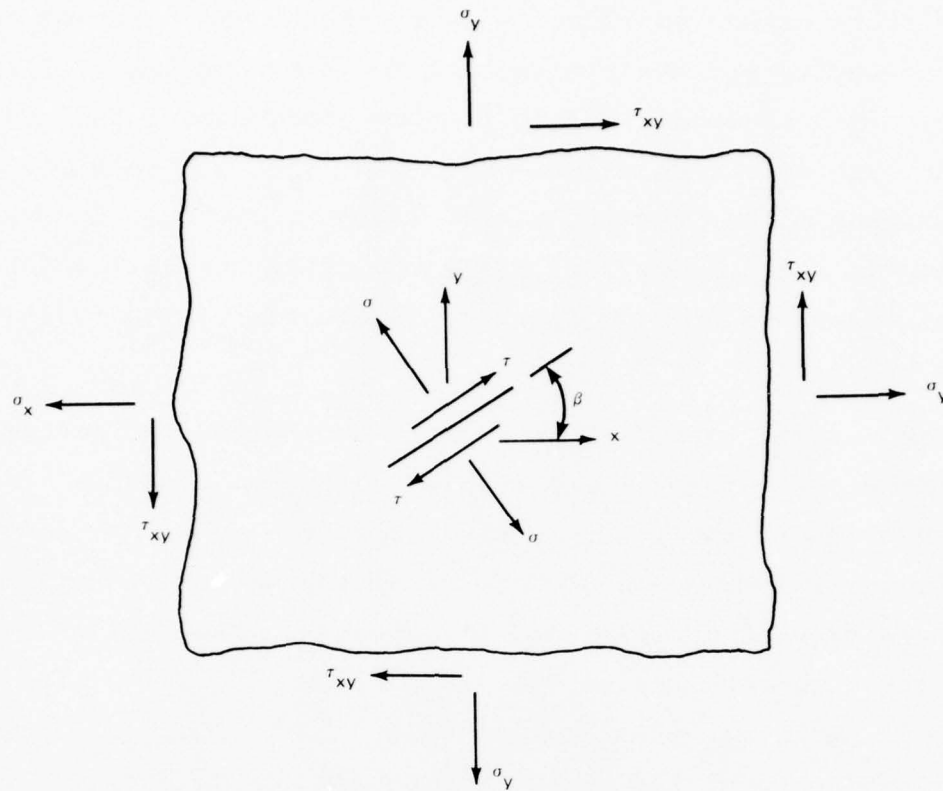
Fig. 3 Crack in a Biaxial Stress Field

$$\sigma = (\sin^2\beta)\sigma_x + (\cos^2\beta)\sigma_y + (2\sin\beta\cos\beta)\tau_{xy} \tag{42}$$

$$\tau = (\sin\beta\cos\beta)(\sigma_x - \sigma_y) + (\cos^2\beta - \sin^2\beta)\tau_{xy} \tag{43}$$

where $\sigma_x, \sigma_y, \sigma_{xy}$ are the coordinate stress components, and β is the angle between the crack and the x-axis. The values of the applied elastic stress intensity factors can then be calculated, using Eqs. (42) and (43), and Table 2 as

22

$$K_1 = \alpha \sqrt{2b \; \tan(\pi a/2b)} \left[(\sin^2 \beta)\sigma_x + (\cos^2 \beta)\sigma_y + 2(\sin \beta \; \cos \beta)\tau_{xy} \right] \qquad (44)$$

$$K_2 = \alpha \sqrt{2b \; \tan(\pi a/2b)} \left[(\sin \beta \; \cos \beta)(\sigma_x - \sigma_y) + (\cos^2 \beta - \sin^2 \beta)\tau_{xy} \right] \quad (45)$$

where $\alpha = 1.0$ for an interior crack, and 1.12 for an edge crack.

The case of an arbitrarily oriented crack in a known ambient plane stress field has now been reduced to the equivalent case of a crack with known applied mode I and mode II stress intensities. This so-called "mixed mode" fracture has been recently given some attention, with useful results.

The concept that a crack will tend to propagate in a radial direction from the crack tip along which the elastic strain energy density is a minimum, and crack extension in that direction will occur when that local minimum strain energy density equals or exceeds the critical value was introduced by Sih (Ref. 9). This fracture criterion can be stated as

$$\frac{1}{4}(3 - 4\nu - \cos \theta^*)(1 + \cos \theta^*)\left[\frac{K_1}{K_{1_c}} \right]^2$$

$$+ \left[\frac{3}{2}(1 - 2\nu)/\left(1 - \nu - \frac{\nu^2}{2}\right) \right]^{\frac{1}{2}} \sin \theta^*(\cos \theta^* - 1 + 2\nu)\left[\frac{K_1}{K_{1_c}} \right]\left[\frac{K_2}{K_{2_c}} \right]$$

$$\qquad (46)$$

$$+ \left[\frac{3}{2}(1 - 2\nu)/\left(1 - \nu - \frac{\nu^2}{2}\right) \right] \left[(1 - \nu)(1 - \cos \theta^*) \right.$$

$$+ \frac{1}{4}(1 + \cos \theta^*)(3 \cos \theta^* - 1)\left] \left[\frac{K_2}{K_{2_c}} \right]^2 \geq (1 - 2\nu)$$

where ν is Poisson's ratio and θ is the angle measured from a forward extension of the crack line. The angle $\theta = \theta^*$ minimizes the left hand side of Eq. (46), and is the angle of potential crack extension ($\theta^* = 0$ is a colinear extension). An additional and essential condition, explained by Swedlow (Ref. 10) that must be applied is that $\sigma_\theta(\theta^*) > 0$. That is, the hoop stress component normal to the potential crack extension direction must be tensile. This last condition leads to the expression

$$
\left(3 \cos \frac{\theta^*}{2} + \cos \frac{3\theta^*}{2} \right) \left| \frac{K_1}{K_{1_c}} \right|
$$

$$
- 3 \left[\frac{3}{2} (1 - 2\nu) / \left(1 - \nu - \frac{\nu^2}{2} \right) \right]^{\frac{1}{2}} \left(\sin \frac{\theta^*}{2} + \sin \frac{3\theta^*}{2} \right) \left| \frac{K_2}{K_{2_c}} \right| \geq 0
$$

(47)

Equations (46) and (47) were numerically evaluated for this report, using a digital computer. These minimum strain energy theory results are displayed graphically as interaction curves of K_1/K_{1_c} versus K_2/K_{2_c} for various values of ν in Fig. 4.

Note that the curves vary with Poisson's ratio. It can be found from Eqs. (46) and (47), when K_1 and K_2 are applied separately (Ref. 9), that theoretically

$$
\left| \frac{K_{2_c}}{K_{1_c}} \right|^2 = \frac{3}{2} \frac{(1 - 2\nu)}{\left(1 - \nu - \frac{\nu^2}{2} \right)}
$$

(48)

Therefore

$$
\frac{K_2}{K_{1_c}} = \frac{K_2}{K_{2_c}} \left| \frac{K_{2_c}}{K_{1_c}} \right| = \left| \frac{3}{2} \frac{(1 - 2\nu)}{\left(1 - \nu - \frac{\nu^2}{2} \right)} \right|^{\frac{1}{2}} \frac{K_2}{K_{2_c}}
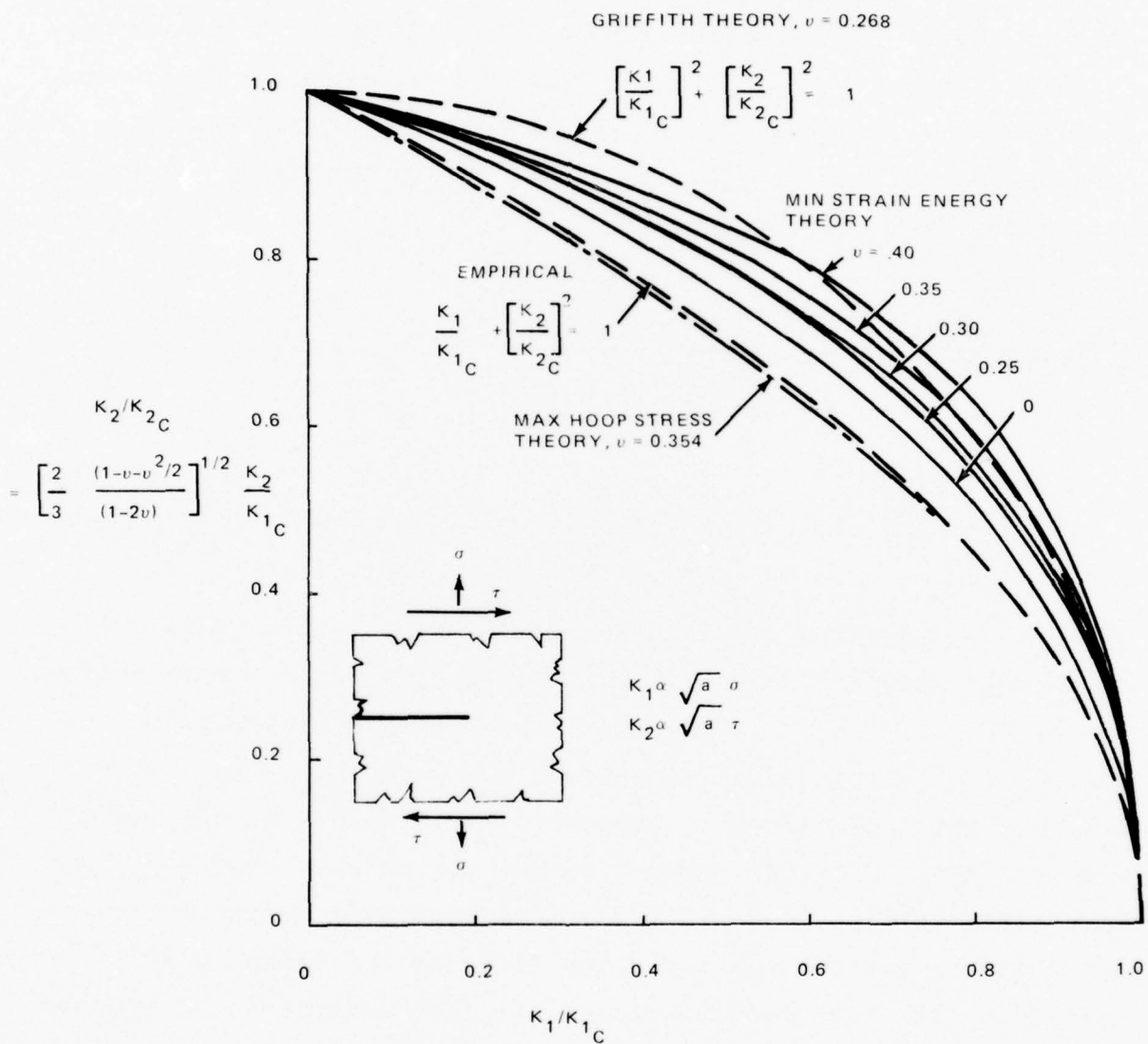$$

(49)

Fig. 4 Mixed-Mode Fracture Theories

Use of K_2/K_{1_c} instead of K_2/K_{2_c} may prove more convenient in applications, since K_{2_c} data are not as commonly available as K_{1_c} data.

An earlier theoretical mixed-mode fracture criterion, from Erdogan and Sih (Ref. 11), states that a crack will tend to propagate in the radial direction from its tip along which the circumferential stress, σ_θ, is a maximum, and crack extension in that direction will occur when that circumferential stress equals or exceeds the critical value. This fracture criterion can then be expressed, incorporating Eq. (49), as

$$\frac{1}{4} \left(3 \cos \frac{\theta^*}{2} + \cos \frac{3\theta^*}{2}\right) \left|\frac{K_1}{K_{1_c}}\right|$$

(50)

$$- \frac{3}{4}\left[\frac{3}{2}\ (1 - 2\nu)/\left(1 - \nu - \frac{\nu^2}{2}\right)\right]^{\frac{1}{2}} \left(\sin \frac{\theta^*}{2} + \sin \frac{3\theta^*}{2}\right) \left|\frac{K_2}{K_{2_c}}\right| \geq 1$$

where θ^* minimizes the left hand side of Eq. (50). This criterion was also evaluated for this report for various combinations of K_1/K_{1_c} and K_2/K_{2_c}. However, the resulting interaction curves do not, in general, intersect the point $K_2 = K_{2_c}$ when $K_1 = 0$, which condition is theoretically required by the definition of K_{2_c}. Only one curve does so, for which $\nu = 0.354$, and this curve is plotted in Fig. 4. Note that this particular value of Poisson's ratio is at the upper limit of the range $0.29 < \nu < 0.35$, pertaining to most structural metals. The corresponding interaction curve for the lower limit of $\nu = 0.29$, a typical value for steels, has the K_2/K_{2_c} values uniformly reduced by 17 percent. For $\theta = 0.33$, a typical value for aluminum, the reduction of K_2/K_{2_c} values is only 5 percent, compared to the curve shown.

26

An older theoretical mixed-mode criterion is an extension of the classical Griffith-Irwin theory (Ref. 12), that assumes the crack will always tend to extend in its current direction $(\theta^* = 0)$, regardless of the relative values of K_1 and K_2, and the energy release rates of the two modes calculated separately can then be merely added algebraically. The mixed-mode fracture criterion is then

$$\left[\frac{K_1}{K_{1_c}}\right]^2 + \left[\frac{K_2}{K_{1_c}}\right]^2 \geq 1 \tag{51}$$

Using Eq. (49), this becomes

$$\left[\frac{K_1}{K_{1_c}}\right]^2 + \frac{3}{2} \frac{(1 - 2\nu)}{\left(1 - \nu - \frac{\nu^2}{2}\right)} \left[\frac{K_2}{K_{2_c}}\right]^2 \geq 1 \tag{52}$$

This criterion also generally fails to satisfy the requirement that $K_2 = K_{2_c}$ when $K_1 = 0$, except for $\nu = 0.268$, for which $K_{2_c} = K_{1_c}$. The interaction curve for this particular value of Poisson's ratio is plotted in Fig. 4. For $\nu = 0.29$, the values of K_2/K_{2_c} are 14 percent larger than shown in the curve, making this curve less conservative for the practical values of ν. Among the theories discussed, only the modified minimum ϵ energy criterion satisfies the theoretical conditions of variable θ^* and $K_2 = K_{2_c}$ when $K_1 = 0$.

Finally, two empirical interaction formulas were examined. Wu (Ref. 13) has reported the interaction formula

$$\frac{K_1}{K_{1_c}} + \left[\frac{K_2}{K_{2_c}}\right]^2 \geq 1 \tag{53}$$

27

based on test data with orthotropic materials such as wood and glass fiber reinforced plastic. His curve is plotted in Fig. 4 and falls close to the special case of the maximum hoop stress theory for $\nu = 0.354$, and is somewhat conservative compared to the minimum strain energy curves.

Palaniswamy and Knauss (Ref. 14) extended the Griffith theory without the restriction of colinear ($\theta^* = 0$) crack extension. They assumed that the crack would tend to extend in a direction for which the energy release rate was a maximum, and crack extension would begin when that energy release rate equaled the crack surface formation energy. Their numerical solutions agreed well with their test results on a very brittle isotropic (swollen polyurethane elastomer) material, and led them to propose the interaction formula

$$\frac{K_1}{K_{1_c}} + \frac{3}{2}\left[\frac{K_2}{K_{2_c}}\right]^2 \geq 1 \tag{54}$$

which, in effect, reduces all the allowable values of K_2 from Eq. (53) by 18 percent. This formula fails to give $K_2 = K_{2_c}$ at $K_1 = 0$, for any Poisson ratios and therefore Eq. (54) is not plotted in Fig. 4.

At this point it should be mentioned, as indicated by Swedlow (Ref. 10), that both the minimum strain energy density theory and the maximum hoop stress theory indicate "weak" tendencies toward their predicted values. That is, in many mixed-mode cases, the variation of induced strain energy density or hoop stress is often small near the crack tip, so that there will be a tendency for small local variations in material properties to alter the crack direction and induce scatter in the measured data. Therefore, small

28

differences between various theoretical predictions should not be important.

In conclusion, it appears that the empirical interaction curve of Eq. (53) would be the best choice at present, because it is a simple formula that is moderately conservative compared to the modified minimum strain energy theory. This phenomenon is the object of considerable study among engineering researchers and further clarifications should be available in the next few years.

The equations shown here do not apply when the crack is in a region of gross plasticity induced by the external loads. However, in that case, the critical condition for the element "failure" will probably be ductile rupture/tearing or plastic collapse and not fracture. In a highly redundant structure with multiple load paths, an element with a flaw or crack will either fail by fracture or yield plastically, but probably not both. Both fracture and rupture/tearing failures cause complete shedding of load, while gross plasticity causes shedding of additional load to the surrounding elements.

For example, a thin skin panel section of width $2b = 10$ in. in uniaxial tension has a presumed flaw or crack transverse to the applied stress of length $2a = 0.10$ in. The material has a (0.2 percent offset) yield strength of 100 ksi and a mode I fracture toughness, measured for its particular thickness, of $k_{1_c} = 30$ ksi in. The critical level of applied stress is calculated from Table 2, as

$$\sigma_{cr} = K_{1_c} / \sqrt{2b \, \tan(\pi a/2b)} \approx 200 \text{ ksi tension}$$

This value is twice the yield strength and will not be reached in any redundant structure containing this component. The component will become grossly plastic first, losing most of its initial stiffness and dumping any additional load into adjacent stiffer (less

29

plastic) structural components. Thus, although the fracture analysis was not applicable in this case, it was not needed either, since gross yielding was the critical condition. If the presumed crack was sufficiently longer, or the K_{1c} smaller, or the yield strength larger, then the critical stress for fracture would have been in the elastic range. The formula in Table 2 would have then been applicable, and the element(s) containing the crack would have "failed" by fracture. These elements would then have been completely removed from the load path by reducing their stiffness to zero, dumping all their load into adjacent elements.

CONNECTION FAILURES

The behavior of connections and joints during large plastic deformation might have a significant effect upon the gross deformations and energy absorption of the entire structure. Strong, rigid joints will probably cause plastic "hinges" to be formed in the adjacent elements, when the loads and deformations are sufficiently large. On the other hand, ductile joint fittings may themselves account for a significant amount of energy dissipation and deformation. In any case, complete joint failure will have a great effect on the local load distribution. Future applications of the theory and comparison with test data should determine the real importance of joint behavior in a crash or crush event.

In the conventional structural analysis, idealized perfect joints are assumed to be present. These perfect joints are points (nodes) in the structure, rigidly connecting two or more components, such that certain specified relative deformations between the components are completely restrained while transferring unlimited loads. However, real joints can have the following characteristics:

30

- Slip - deformation at zero load

- Elasticity - small recoverable deformation under load

- Yield - large nonrecoverable deformation under load

- Failure - complete load loss followed by free deformations

Slip is not usual in aircraft construction, but is possible in poorly made joints or in special cases of initially "soft" joints. Elastic deformation of the connection fittings is usually small relative to the total structural deformation. Yield rotations at joints should have a noticeable effect on the structure, but tension and shear yielding could also be a factor. Every real joint will have a failure load, or critical combination of load components.

Consider first the relationship between any one component of relative motion at a joint and its corresponding load component, assuming that no other loads are imposed. This is a joint having restraint in only one degree-of-freedom. Three types of joint behavior are defined for the joint failure criteria. They are shown schematically in Fig. 5 and are:

- Type 1 - Rigid unbreakable joint. No deformation, unlimited load capacity, no energy absorbed.

- Type 2 - Rigid breakable joint. No deformation up to failure load, followed by complete sudden loss of load, then no resistance to deformation. No energy absorbed. Specify only failure load as input.

31
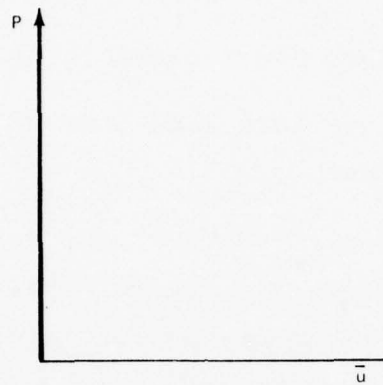
a) Type 1 - Rigid, Unbreakable
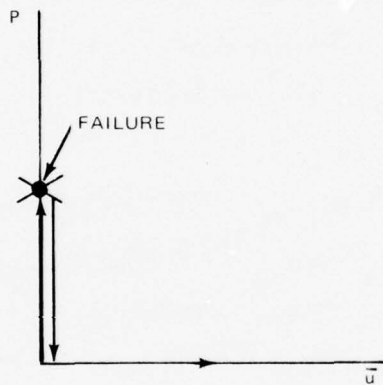
b) Type 2 - Rigid, Breakable

c) Type 3 - General

Fig. 5 Joint Behavior Characteristics

32

- Type 3 - Deformable breakable joint. Can have slip, elasticity, yielding, and failure. Specify load deformation curve up to the failure point. When both the failure load and failure deformation have been reached or exceeded, the load drops to zero suddenly at constant deformation, followed by no resistance to deformation. Finite energy absorbed.

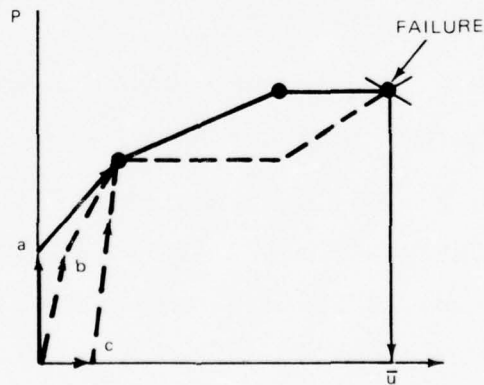In the finite element method used in DYCAST, the loads are calculated only at nodal points. Therefore, the idealization should be arranged such that nodal points are at all the connections to be monitored. At those connection points double nodes should be used, one node on each of the connected elements, at the same location in the structure. This will allow relative displacements and rotations between the nodes to be treated in the incremental equations of motion.

Rigid Breakable Joint

For this type of joint, the two coincident nodal points on the attached elements are effectively tied together until a failure condition is met or exceeded. That is, certain components of motion of one node of the pair are made effectively equal to those of the other node. However, when the critical load is reached, the nodal loads across the joint are reduced to zero, and those motion components of the two nodes are made effectively independent for subsequent time increments.

This might be implemented in the program in two ways. In the method of variable constraints, the restrained degrees-of-freedom (DOF's) for one node of the pair can be initially set equal to those of the other node. When the failure condition is met, those previously

33

dependent DOF's would be made independent and added to the solution variables. This procedure involves relaxing the restraint conditions on some of the nodes, thereby increasing the number of solution variables, in the middle of the problem. The load components in the direction of failure could be reduced to zero (unloaded) over a few time steps preceding the change, to reduce numerical difficulties.

In the method of variable stiffness, the coincident nodes would have independent DOF's during the entire problem, with the nodes connected by springs having infinite (or very large) stiffness components prior to failure. At failure, certain stiffness components are reduced to zero (or made very small). In this way, the total number of DOF's would remain constant throughout the analysis. This is a special case of the treatment of a Type 3 (deformable) joint, described later. The stiffness could be reduced over several time steps, if necessary, to reduce numerical problems.

It seems that the latter method of implementing the failure would be better on the grounds that the number of solution variables would remain constant, and that the behavior of both types of breakable joints are formulated in the same way.

The simplest connection failure criterion is one in which complete joint failure will occur when any one load component reaches its known failure level. This noninteractive joint failure criterion is expressed as

$$\frac{P_i}{P_{i_f}} \geq 1 \tag{55}$$

where P_i is any applied load or moment component and P_{i_f} is the corresponding failure level of the joint when that component is applied alone.

34

However, the critical value of one load component is often reduced when other components are applied. In general, failure of fasteners under combined loads has been characterized by interaction equations of the type

$$\left(\frac{P_1}{P_{1_f}}\right)^{n_1} + \left(\frac{P_2}{P_{2_f}}\right)^{n_2} + \left(\frac{P_3}{P_{3_f}}\right)^{n_3} + \ldots > 1 \tag{56}$$

where the values of n_i depend on the particular application. Some connections have as many as six simultaneously applied load and moment components.

In the particular case of transverse shear load S and axial tension T, failure of fasteners has been characterized by the interaction equation

$$\left(\frac{S}{S_f}\right)^2 + \left(\frac{T}{T_f}\right)^2 > 1 \tag{57}$$

or more accurately, according to Ref. 7, Chapter 8, by the empirical equation

$$\left(\frac{S}{S_f}\right)^3 + \left(\frac{T}{T_f}\right)^2 > 1 \tag{58}$$

These two equations are plotted in Fig. 6. Equation (57) is up to 17 percent more conservative (smaller allowable load components) than Eq. (58) for linear elastic cases. Other interaction formulas are in use with larger exponents, but are less conservative than Eq. (58). As the exponents approach infinity, the two loads become independent, and the failure condition is

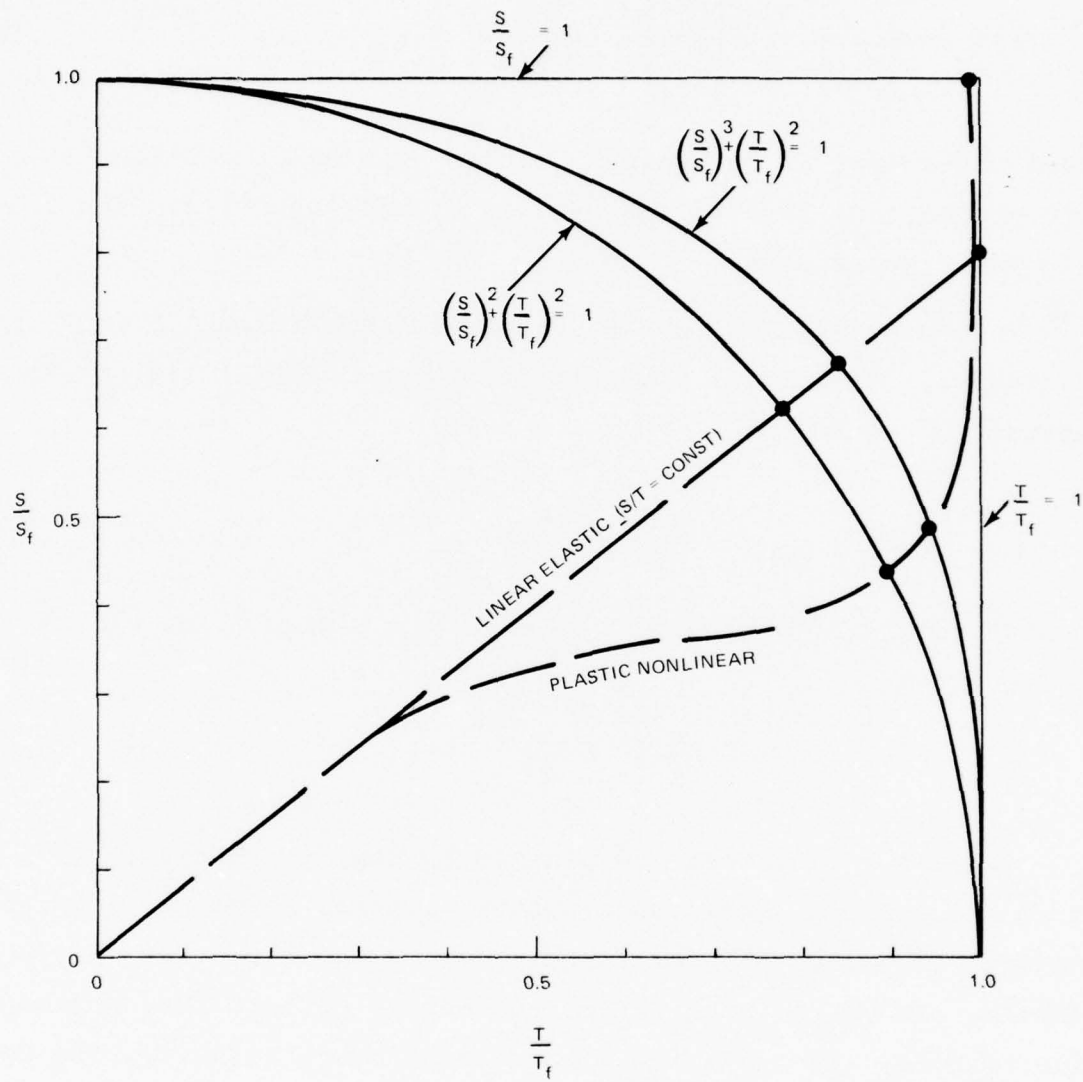$$\frac{S}{S_f} \geq 1 \quad , \quad \frac{T}{T_f} \geq 1 \tag{59}$$

35

Fig. 6 Failure Curves for Two Combined Loads

36

as shown by the limiting "square curve" in Fig. 6. This is the uncoupled failure criteria of Eq. (55), applied to a two degree-of-freedom restrained joint. This criterion might be easier to use than the others, but it is always nonconservative. For nonlinear structural behavior the loads do not necessarily follow any fixed ratio, and the failure point using Eq. (59) can be at much greater loads than allowed by Eq. (58). This is shown in Fig. 6 by the dashed load path for an unusual, but possible, nonlinear case.

Extending Eq. (57) to the general case of a six degree-of-freedom restrained joint, it seems that an interaction formula of the type

$$\sum_{i=1}^{6} \left(\frac{P_i}{P_{i_f}}\right)^2 \geq 1 \tag{60}$$

might be a useful approximation for a conservative failure criterion. On the other hand, Eq. (55) would probably be the upper bound on failure. Both of these could be incorporated into DYCAST, with Eq. (60) to be used automatically unless Eq. (55) was specified.

For line joints and seams (rivet lines, bolt lines, spot welds, seam welds, and adhesive bond lines), the failure criteria can be used by replacing the point loads P_i by N_i, the loads per unit length. For discrete fastener linear joints such as rivet, bolt, and spot weld lines, the failure loads per unit length could be computed by dividing the unit fastener failure load (as given in Ref. 7, Chapter 8, for example) by the fastener spacing. In some cases, the use of discrete fasteners will reduce the local tension strength of the parent sheet material because of the holes,

37

and this should be taken into account. Reference 7 gives such information for spot welds.

In the application of the joint failure criterion, double nodes are required for each element pair to be separated. An example of a stringer attached to a skin panel is shown in Fig. 7. Prior to failure, there are ten elements (eight membrane triangles and two stringer elements) connected to a single node point, as in Fig. 7a. Two failure modes at the same point are permitted in this example, since the stringer can tear away from both skin panels separately. Thus, as shown in Fig. 7b, three initially coincident nodes would be required, node A connecting the left set of membrane triangles, node C connecting the right set, and node B for the stringer elements. Since the membrane elements permit only in-plane loads, the membrane load components (in the stringer's local coordinate system) are tension and shear at nodes A and C. The failure criterion Eq. (60) reduces to the two component version Eq. (57), and can be applied separately for each of the node pairs AB and BC. Note that $P_x^A = P_x^C$ and $P_x^B = 0$ for this particular example because the stringer carries no transverse loads. However, $P_y^A \neq P_y^C$, so that failure of the left and right node pairs can occur at different times. Specifically, after one side fails, $P_x^A = P_x^C = 0$, and then the other side can fail in shear alone.

If the joint failure is to be handled by the variable stiffness method, the three nodes would be separately specified at the start. The four stiffness components connecting the node pairs (one tension and one shear per node pair), must be also initially specified. Only the extensional "springs" for nodes AB and BC are shown in Fig. 7. These stiffness components are initially set very large to rigidize the joint connections in the extension and shear modes. After
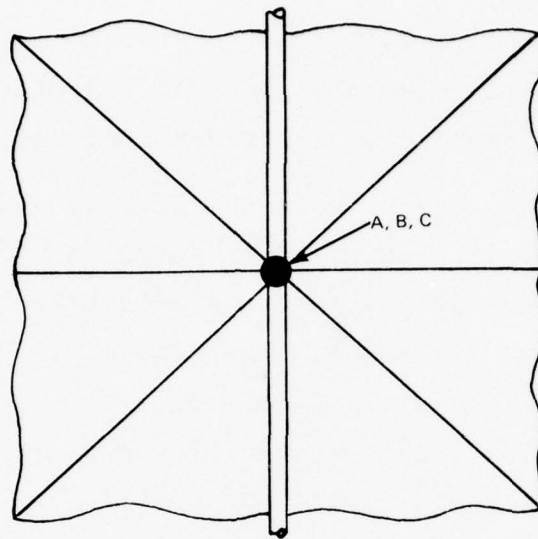
a) Typical Multiple Element Joint (Pre-Failure)
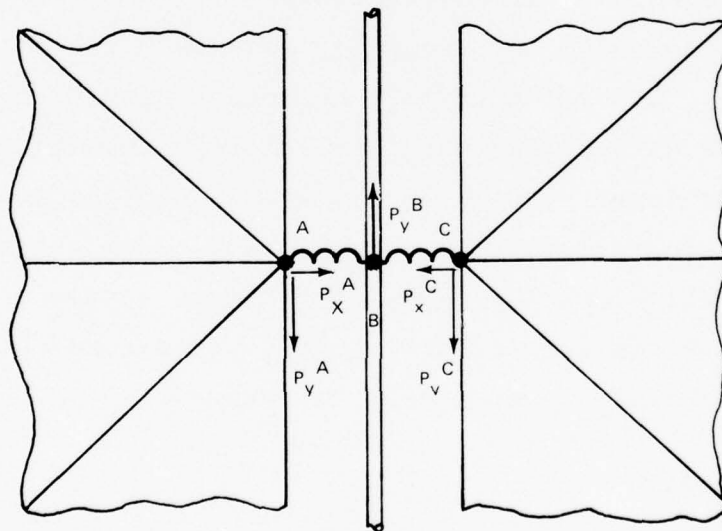
b) Admissible Post-Failure Deformations

Fig. 7 Skin - Stringer Joint Failure Model

failure, these stiffness components are reduced to zero (or nearly zero), allowing free motions of the specified displacement components.

Note that no failure is permitted for the other element combinations among the ten elements, because the necessary separate nodes and nodal stiffness components were not specified.

In the case of joints between the beam and plate elements, which permit moments and out-of-plane forces at the nodes, the failure specifications are similar but with more stiffness components per node. For the beam element, there are six components per node, and five for the plate element. The four element types in DYCAST, their nodal load components, and their interactive failure criteria are given in Fig. 8.

In general, the failure load components at a joint will be determined experimentally or calculated from known test data (Ref. 7, Chapter 8, for example), conveniently oriented with respect to the joint geometry. The joint failure component directions will not always coincide with either the local element coordinate system or the global coordinate system, in which the load components are calculated. Therefore, provision must be made to either transform the failure components into the global coordinate system for the application of the joint failure criteria, or to transform the load components into the failure component directions.

Deformable Joints

This type of joint has the character of a structural element, since it carries load while permitting deformation between connection points. It is a special element in that it has no finite dimensions, since the two nodes it connects in the structure are at a single

40
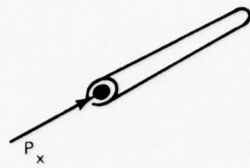
a) Stringer Element (1 Component)
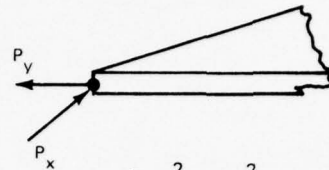
$$\left(\frac{P_x}{P_{x_f}}\right) \geqslant 1$$

b) Membrane Element (2 Components)

$$\left(\frac{P_x}{P_{x_f}}\right)^2 + \left(\frac{P_y}{P_{y_f}}\right)^2 \geqslant 1$$

c) Beam Element (6 Components)

$$\left(\frac{P_x}{P_{x_f}}\right)^2 + \left(\frac{P_y}{P_{y_f}}\right)^2 + \left(\frac{P_z}{P_{z_f}}\right)^2 + \left(\frac{M_x}{M_{x_f}}\right)^2 + \left(\frac{M_y}{M_{y_f}}\right)^2 + \left(\frac{M_z}{M_{z_f}}\right)^2 \geqslant 1$$

d) Plate Element (5 Components)

$$\left(\frac{P_x}{P_{x_f}}\right)^2 + \left(\frac{P_y}{P_{y_f}}\right)^2 + \left(\frac{P_z}{P_{z_f}}\right)^2 + \left(\frac{M_x}{M_{x_f}}\right)^2 + \left(\frac{M_y}{M_{y_f}}\right)^2 \geqslant 1$$

Fig. 8 Nodal Load Components and Joint Failure Criteria

41

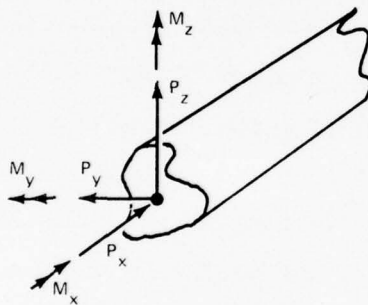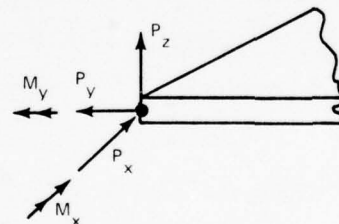geometric point. Furthermore, its variable stiffnesses do not have to be calculated as in the usual finite element, but are input as data. This joint element is therefore similar to a beam/ spring element used in the traditional lumped mass-spring models, but with zero length.

The recommended procedure for a deformable joint would be to input a table of load and deflection values describing a linear-segmented curve such as in Fig. 5c, with one such curve for each restrained deformation component, to be used in forming the instantaneous stiffness matrix for that joint element. The joint deformation then becomes a special elastic-plastic element, whose stiffness can be simply extracted from the input data, instead of being calculated by integration over the element volume, as in the normal finite element.

The deformable joint permits various behaviors to be represented as in Fig. 5c. The solid curve shows an expected input, with initial rigidity to point a, followed by progressive loss of stiffness to the failure point. Shown by the dashed curves are cases with initial elasticity to point b, and initial slippage to point c. Flat (zero stiffness) load deformation segments should be permitted as shown, but negatively sloped segments should not, because of instability problems.

This deformable joint requires that the joint stiffness components and deformation components be added to the problem formulation from the start. Each node of the connected pair will then have its own set of displacements, rotations, forces, and moments. The nodal loads will have to be transformed into vector components that are compatible with the specified critical load vector for the element. These loads are shown in Fig. 8 for the four element types used in DYCAST. The maximum number of loads specified for any joint node is six.

42

The most general pair of joint nodes would then have 12 restrained degrees-of-freedom associated with it. These are the three displacements and three rotations for each node of the pair. There are then six components of relative motion that are related in some way to the six corresponding components of load (three forces and three moments). In a completely coupled joint there would then be 36 variable stiffness functions between all the load and relative motion components of which only 21 would be independent. If we admit for consideration only the direct relations between a particular relative motion component and its corresponding load component, neglecting the coupling between different component directions, there remains only six load-motion functions. For example, longitudinal force versus relative longitudinal displacement, and torque versus relative rotation about the longitudinal axis are allowed, but force versus rotation or torque versus longitudinal displacement are not allowed.

This elimination of coupling or interaction at the joints is probably a gross simplification of the actual joint behavior, but is considered necessary for a first step practical attempt to incorporate a joint deformation model into the structural code. The uncoupled joint model also allows simpler tests to determine stiffness functions. A coupled nonlinear deformation model prevents simplified tests, since the ratio of the various load components would vary depending upon the particular crash conditions, and could not be determined beforehand.

The static incremental load-deformation behavior of the joint is then simply characterized by a variable diagonal stiffness matrix K, where

$$\Delta F_i = K_{ii} \Delta \overline{U}_i \quad ; \quad i = 1, 2, \ldots, 6 \tag{61}$$

43

where F_i are the nodal load components, $\bar{U}_i = U_{i_2} - U_{i_1}$ are relative nodal deformation components (U_{i_1}, U_{i_2} are the absolute deformation components of nodes 1 and 2 of the joint pair), and the stiffness components K_{ii} are the current slopes of the individual load components versus deformation component curves, that were input as in Fig. 5c. Equation (61) is shown in its simplest form, corresponding to the most convenient local coordinate system at the joint. A transformation into the global coordinate system would be done to incorporate the joint deformation into the solution.

Some joints will not require all six stiffness components. For example, a shear pin, bolt, or wing pivot fitting will allow free rotations about one axis (neglecting friction), leaving five nonzero stiffness components. But the two shear stiffnesses in the plane of rotation will probably be equal, as well as the two bending stiffnesses transverse to that plane; this leaves only three independent stiffness coefficients; axial tension, in-plane shear, and transverse bending. Any stiffness component may arbitrarily be made very large to effectively eliminate a joint deformation component. Likewise, the corresponding failure load component can be made very large to eliminate its failure mode.

Other joints will not admit all six components because the connected elements do not permit six load components per node. In DYCAST only the beam element has all six components per node, as shown in Fig. 8.

In the case of linear deformable joints such as rivet lines, bolt lines, welds, adhesive bond lines, etc., the behavior is most conveniently described by plotting the distributed load component N_i (load per unit length) versus the deformation component U_i, in

44

the same manner as in Fig. 5c. This form is the most meaningful
for displaying test data. The incremental load-deformation equa-
tion is then

$$\Delta N_i = k_{ii} \Delta \overline{U}_i \tag{62}$$

where k_{ii} is the current distributed stiffness component of the
joint in load per unit deformation per unit length, equal to the
current slope of the N_i versus $\overline{U}_i$ input data curve.

The program requires that a unique relationship between the
nodal forces and deformation components be established, so that
Eq. (62) must be transformed into the form of Eq. (61). An equiva-
lent set of nodal forces must be devised, with an effective nodal
stiffness K_{ii} calculated from the distributed stiffness k_{ii}.
One arbitrary way would be to assume that the forces at a given node
are uniformly distributed along the joint line from a point halfway
to the node on one side to a point halfway to the node on the other
side, as shown in Fig. 9. The concentrated and distributed nodal
forces are then related by

$$N_n = 2F_n / (d_{n-1} + d_n) \tag{63}$$

where n indicates a special internal node number sequence of the
linear joint, from node 1 to node N, and d_n is the nodal spacing.

For a noncontinuous or "finite" joint that starts and ends at
different points, the end loads can be obtained from Eq. (63) by
setting $d_o = d_1$ and $d_N = d_{N-1}$. This is equivalent to creating
fake segments outside the end nodes, equal in length to the end
segments. In the case of an "endless" joint line, such as a com-
plete circumferential joint around the fuselage at a frame, the
starting and ending node will be the same. Across the common start-
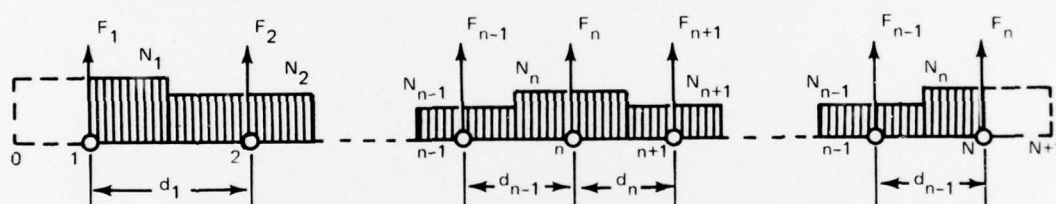finish node, at $n = 1$, set $d_o = d_N$ in Eq. (63).

Fig. 9 Distributed Loads at a Linear Joint

Now Eqs. (62) and (63) result in

$$\Delta F_{in} = \tfrac{1}{2}(d_{n-1} + d_n)k_{ii_n}\Delta\overline{U}_{in} = K_{ii_n}\Delta\overline{U}_{in} \tag{64}$$

for the component index $i = 1, 2, \ldots, 6$ and the node index $n = 1, 2, \ldots, N$. Thus, the current effective nodal stiffness component K_{ii_n} is

$$K_{ii_n} = \tfrac{1}{2}(d_{n-1} + d_n)k_{ii_n} \tag{65}$$

Equation (65) permits the line joint to be treated as an equivalent set of nodal joints using Eq. (61).

The different treatment between an endless and a finite joint line could be handled at the input. The node numbers comprising the joint should be entered in their proper sequential order as they appear along the joint. The endless joint line will have the same first and last node number. The values of d can be calculated from the input coordinates of adjacent nodes. Then, Eq. (65) will be used with $d_o = d_N$ when $n = 1$. The finite joint line will have different end node numbers, and then Eq. (65) will be used with $d_o = d_1$ and $d_N = d_{N-1}$.

The failure of the deformable joint might be treated by merely assuming that failure occurs when any one relative deformation component reaches or exceeds its failure value. This would be analogous to the noninteractive failure criterion of Eq. (55), which can overpredict the failure point under combined loads. A more consistent approach would be to require that the last load value of the input load-deformation curve be the failure load value for that component. Then the same failure criteria, Eq. (60) and Fig. 8, can be used as in the rigid breakable

47

joint, described previously. In the case of a failure that occurs after a flat load deflection segment (solid curve in Fig. 5c), an artificial, very short segment with a small final load increase would define a unique failure point, without a significant loss of accuracy.

As before, all the stiffness components of the failed joint would be reduced to zero (or very small values) when its failure criterion was satisfied. The sudden change in some stiffness components will induce transient dynamic effects (stress waves, vibrations) that may affect the numerical operations (requiring a smaller time step during the transient) and the stability of the structure. Changing the stiffness values over several time steps might reduce these transient effects.

3. DEFORMATION FAILURES

PLASTIC COLLAPSE

Failure modes involving purely plastic collapse of structural members are automatically incorporated into the calculations. Consider a hypothetical material possessing unlimited ductility with no failure point. As the stress increases, the strain can eventually increase without limit. Structural components or elements made of such materials will develop one of the load deformation curves shown in Fig. 10, having potentially unlimited deformation and energy dissipation. As the plastic regions in a member grow in size, the effective stiffness of the member will eventually be reduced, and each load increment will produce a greater deformation increment than before. A point may be reached in which the effective stiffness equals
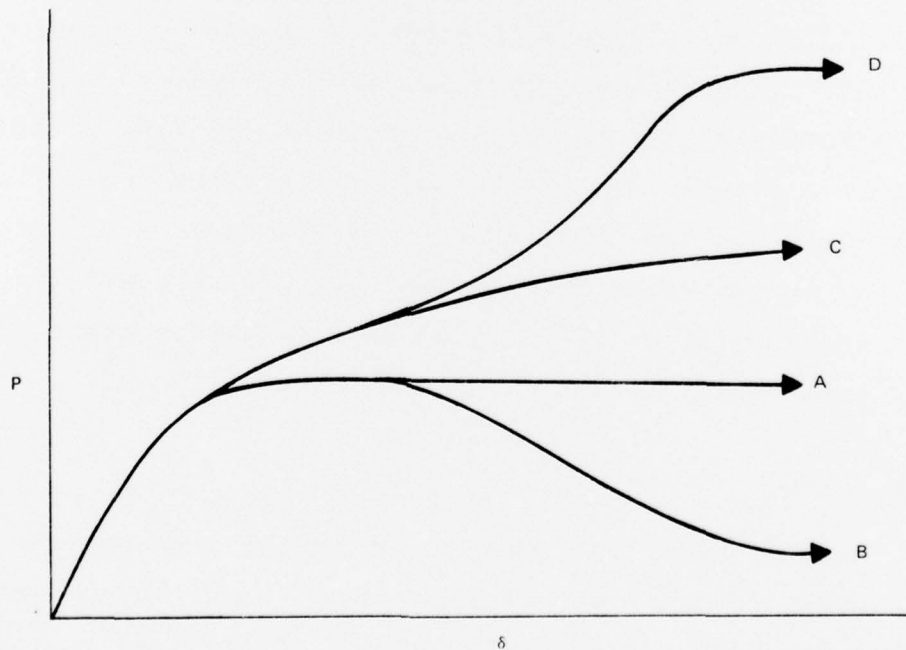
Fig. 10 Plastic Collapse Characteristics

or is sufficiently close to zero (horizontal tangent). A plastic collapse will then occur, in which the deformation proceeds at constant or reducing load, on curves A or B, depending on the load and deformation constraints on the member. On curve C the stiffness has not vanished, but becomes sufficiently small so as to be arbitrarily considered a plastic collapse state. On curve D the stiffness was initially reduced by one deformation mode (plastic bending, for example), then increased at large deformations (by in-plane stretching, for example), until finally collapse occurs when a sufficient volume of the element becomes highly plastic.

In any case, large amounts of energy may be absorbed by the component after reaching the peak load. Real structural materials do not exhibit unlimited ductility, but will suffer a material failure at some point that will limit the total energy absorption. The effects of material failure and the failure criteria were discussed previously (Section 2).

Included in the category of plastic collapse is plastic buckling, in which gross plasticity appears, followed by steadily increasing deformation, approaching a condition of zero stiffness at or near some theoretically predictable instability load. This behavior exhibits the same characteristics as curves A, B, or C in Fig. 10, and is therefore included as part of the elastic-plastic analysis. No special calculation of an instability state is required in this case.

ELASTIC BUCKLING

This type of behavior is characterized by a sudden, "snap-through" change from one deformation state to another. Mathematically, this has been termed "bifurcation" instability because of the existence of two distinct equilibrium deformation states at

50

the same load. The buckled state has a subsequent load deformation path that requires less energy, with lower stiffness and greater deformation, than the initial unbuckled shape.

This type of instability is different from plastic and progressive collapse in the presence of large initial imperfections, or transverse loading, in which deformations increase steadily at ever increasing rates. These latter cases are calculated by the existing plasticity and geometric nonlinearity features in the code.

The sudden elastic buckling of components is not now calculated in DYCAST for the stringer and membrane triangle element, because the bifurcation mechanism is not incorporated in these elements. For example, in the case of a stringer element under compression, the only deformation accounted for is axial compression. Since buckling takes place in the transverse direction involving bending stiffness, this instability mode will not be considered in the existing analysis. The same argument applies for the transverse buckling of panels composed of membrane triangle elements.

Buckling can be calculated using beam and plate elements, which contain transverse deformation components and bending rigidities. However, these elements require many more degrees-of-freedom, and it would be prohibitively expensive to analyze an airplane structure by replacing all the membrane skins and stringers with plates and beams, just to account for buckling that might not occur.

At this point in the development and application of DYCAST, it seems more reasonable to select in advance a limited number of components or subassemblies likely to buckle elastically, and to give them special treatment. This treatment could be to use all bending-type elements (beams and plates) for these components. Another method would be to use all membrane elements, calculating buckling loads in

51

advance, deciding when buckling has occurred, and arbitrarily assign-
ing a post-buckle behavior.

The latter method will require interaction formulas for buck-
ling under combined loads. The configurations of the components or
subassemblies are too varied, covering stiffened and unstiffened
panels, orthotropic panels, honeycomb sandwich panels, etc., to be
explicitly listed here. Many cases have been theoretically and ex-
perimentally researched, and their buckling interaction curves ap-
pear in the open literature. A particular important case of inter-
est in DYCAST is the rectangular panel under biaxial compression
and shear loads. The buckling condition for an unstiffened iso-
tropic plate in that case is

$$\frac{N_x}{N_{x_f}} + \frac{N_y}{N_{y_f}} + \left|\frac{N_{xy}}{N_{xy_f}}\right|^2 \geq 1 \qquad (66)$$

where N_x, N_y, and N_{xy} are the applied values of the two com-
pressive loads and the shear load per unit width, and the subscript
f indicates the failure value when any component is applied alone.
This formula is sometimes used in cases of stiffened, orthotropic,
and sandwich plates. Although not correct for these nonisotropic
cases, the formula is usually conservative (see Ref. 7, Chapter 1,
for example). In any case, three buckling loads must be calculated
for each structural component or assembly of components to be moni-
tored for buckling, and this can become a lengthy process.

After buckling occurs, a post-buckling behavior must be speci-
fied. Typical post-buckling actions are sketched in Fig. 11. The
drop-off in load that is typical of some deeply curved plates and
shells can vary greatly from 90 percent for an unstiffened iso-
tropic thin cylinder under axial compression, to almost nothing for
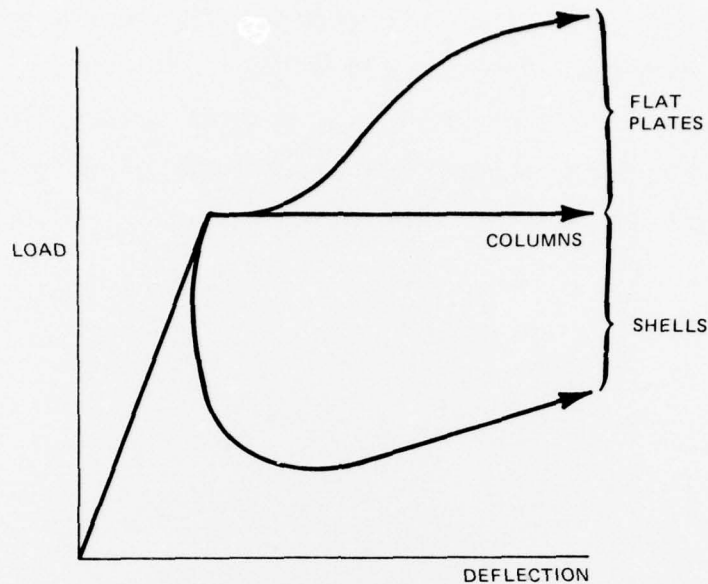
52

Fig. 11 Post-Buckling Characteristics

certain highly orthotropic, or strongly stiffened shells. Most ap-
plications for aircraft structures will be for the flat or nearly
flat plate or panel structures that behave as either plates (with
side support) or wide columns (no side support). Many stiffened
panels show an increase in load carrying ability after initial buck-
ling of the skin because the stiffeners and adjacent skin do not
buckle but deform plastically at higher loads. In cases of general
instability, where the stiffeners and sheet buckle together, a col-
lapse condition can develop with a nearly flat load-deflection curve
as for the column.

Thus, for most aircraft applications, a reasonably conservative
post-buckling model would hold the loads fixed at the buckling values,
while allowing unrestrained deformation. The stiffness of the buckled
elements or group of elements would be reduced to very small values in
the incremental equations.

53

It should be recognized that the incorporation of elastic buck-
ling into the crash analysis will exact a high price in either com-
puter time (if bending elements are used) or in human time (if the
buckling criteria are to be input). At this point, there is not
sufficient evidence concerning the importance of elastic buckling
in crash analysis to justify this effort.

4. INTEGRATION INTO PROGRAM

The computational flow of DYCAST is outlined in Fig. 12. As the structure deforms, the element stiffnesses are altered to account for softening of the material due to plasticity (material nonlinearity), and for decreases or increases in the element's membrane and bending stiffnesses due to large deformations (geometric nonlinearity). Geometric nonlinearity is also accounted for at the global stiffness level, when the structure is placed in its new deformed shape for the next time increment, thus accounting for deformations that are large compared to the structural dimensions.

The deformation of joints is treatable as a simple type of plasticity which reduces the stiffness of the joint springs.

Since the failures described in this report will affect the structure by altering the element stiffnesses, they can be handled in the same way as the existing stiffness changes due to geometric nonlinearity. Thus, the failure mode analysis is shown in Fig. 12 at the element stiffness level.

The special case of complete separation of a structural subassembly (wings, tail, etc.) will occur when all of the elements or nodes attaching it to the main structure have failed. This should be handled by stating the critical set of nodes or elements as input, and when an entire set has failed, the job should stop. The user can then examine the data, and can restart the analysis at the point of separation, eliminating the nodes and elements of the separated subassembly from the subsequent calculations by the proper input instructions.
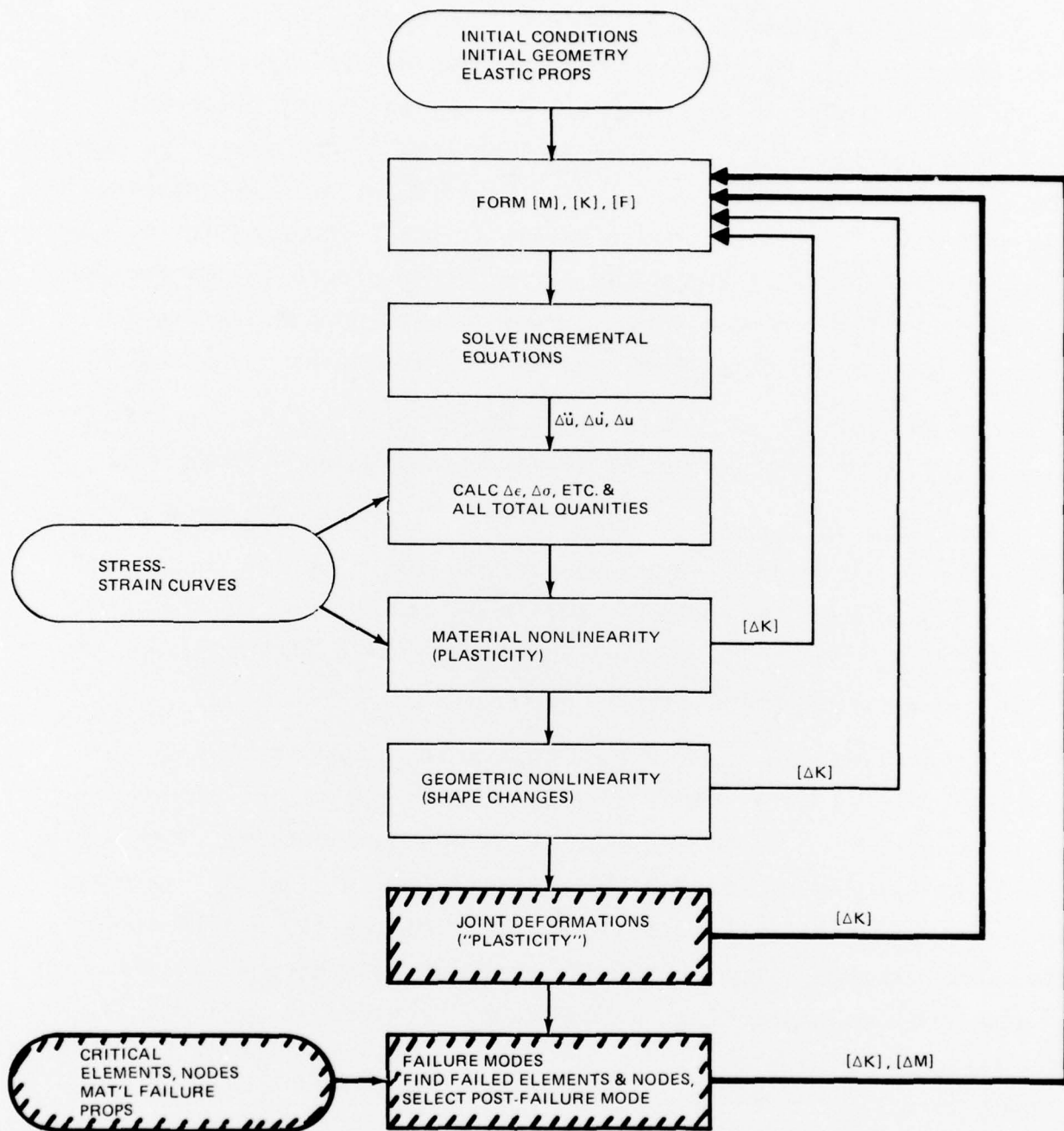
55

Fig. 12 Integration of Failure Modes into DYCAST Flow

5. REFERENCES

1. Pifko, A., Levine, H. S., and Armen, H. Jr., "PLANS - A Finite Element Program for Nonlinear Analysis of Structures. Vol. I — Theoretical Manual," NASA CR-2568, November 1975.

2. Sokolnikoff, I. S., Mathematical Theory of Elasticity, Second Ed., McGraw-Hill, New York, 1956.

3. Burington, R. S., Handbook of Mathematical Tables and Formulas, Handbook Publishers, Sandusky, Ohio, 1957.

4. Love, A. E. H., A Treatise on the Mathematical Theory of Elasticity, Fourth Ed., Dover Publications, New York, 1927.

5. Liebowitz, H., Fracture, An Advanced Treatise, Vols. II - VI, Academic Press, New York, 1969.

6. Paris, P. C. and Sih, G. C., "Stress Analysis of Cracks," ASTM STP 381, American Society for Testing and Materials, Philadelphia, 1970.

7. Military Standardization Handbook, Metallic Materials and Elements for Aerospace Vehicle Structures, MIL-HDBK-5B, U.S. Government Printing Office, Washington, D.C., 15 August 1974.

8. "Standard Method of Test for Plane Strain Fracture Toughness of Metallic Materials," ASTM Standard E399, Annual Book of ASTM Standards, Part 10, American Society for Testing and Materials, Philadelphia, 1975.

9. Sih, G. C., "A Special Theory of Crack Propagation," in Mechanics of Fracture, Vol. 1 - Methods of Analysis and Solutions of Crack Problems, Ed. by G. C. Sih, Noordhoff International Publishing, Leyden, 1973.

10. Swedlow, J. L., "Criteria for Growth of the Angled Crack," in Cracks and Fracture, ASTM STP 601, American Society for Testing and Materials, pp. 506-521, 1976.

11. Erdogan, F. and Sih, G. C., "On the Crack Extension in Plates Under Plane Loading and Transverse Shear," Journal of Basic Engineering, Vol. 85D, pp. 519-525, December 1963.

12. Irwin, G. R., "Fracture Mechanics," in Structural Mechanics, Proc. First Naval Symposium on Naval Structural Mechanics, Ed. by J. N. Goodier and N. J. Hoff, Pergamon Press, London, pp. 557-594, 1960.

13. Wu, E. M., "Application of Fracture Mechanics to Anisotropic Plates," Journal of Applied Mechanics, Vol. 34E, No. 4, pp. 967-974, 1967.

14. Palaniswamy, K. and Knauss, W. G., "On the Problem of Crack Extension in Brittle Solids Under General Loading," Report SM74-8, Graduate Aeronautical Laboratories, California Institute of Technology, 1974.